

Dalton Transactions

Accepted Manuscript



This is an *Accepted Manuscript*, which has been through the Royal Society of Chemistry peer review process and has been accepted for publication.

Accepted Manuscripts are published online shortly after acceptance, before technical editing, formatting and proof reading. Using this free service, authors can make their results available to the community, in citable form, before we publish the edited article. We will replace this *Accepted Manuscript* with the edited and formatted *Advance Article* as soon as it is available.

You can find more information about *Accepted Manuscripts* in the [Information for Authors](#).

Please note that technical editing may introduce minor changes to the text and/or graphics, which may alter content. The journal's standard [Terms & Conditions](#) and the [Ethical guidelines](#) still apply. In no event shall the Royal Society of Chemistry be held responsible for any errors or omissions in this *Accepted Manuscript* or any consequences arising from the use of any information it contains.

To be submitted to *Dalton Trans.*

2/24/2014 10:39 AM

Equiatomic intermetallic compounds YTX ($T = \text{Ni, Ir}$; $X = \text{Si, Ge, Sn, Pb}$): A systematic study by ^{89}Y solid state NMR and ^{119}Sn Mössbauer spectroscopy**Christoph Höting^a, Hellmut Eckert^{*b}, Frank Haarmann^{*c}, Florian Winter^a, and Rainer Pöttgen^{*a}**

^a *Institut für Anorganische und Analytische Chemie, Universität Münster, Corrensstrasse 30, D-48149 Münster, Germany. E-mail: pottgen@uni-muenster.de; Fax: +49 251-83-36002*

^b *Institut für Physikalische Chemie, Universität Münster, Corrensstrasse 30, D-48149 Münster, Germany. E-mail: eckerth@uni-muenster.de; Fax: +49 251-83-29159*

^c *Institut für Anorganische Chemie, RWTH Aachen, Landoltweg 1, D-52074 Aachen, Germany. E-mail: frank.haarmann@ac.rwth-aachen.de; Fax: +49 241-80-92288*

Received ## January 2014, Accepted ## ##### 2014**DOI: #####**

The equiatomic TiNiSi type tetrelides YTX (space group $Pnma$) with $T = \text{Ni, Ir}$ and $X = \text{Si, Ge, Sn, Pb}$ were synthesized from the elements by arc-melting or via high-frequency-melting of the elements in sealed niobium ampoules. All samples were characterized by powder X-ray diffraction using the Guinier technique. The structures of YNiGe , YNiPb , YIrSi , YIrGe , and YIrSn were refined from single crystal X-ray diffractometer data. The YTX tetrelides are characterized by three-dimensional $[TX]$ network that consists of puckered T_3X_3 hexagons with $T-X$ distances in the order of the sums of the covalent radii. YIrSi and YIrGe show a reverse occupancy of the T and X sites with respect to the remaining YTX compounds, which is most likely a size effect. Solid state NMR studies reveal the sensitivity of ^{89}Y Knight shifts to electronic structure details. A monotonic dependence on the tetrelide Pauling electronegativity is observed in addition. The stannides YTSn ($T = \text{Ni, Rh, Ir, Pt}$) were further characterized by ^{119}Sn Mössbauer spectroscopy. They show single signals that are subjected to quadrupole splitting. Comparison of the isomer shifts with the whole series of YTSn stannides gives

no hint for obvious correlations as a consequence of the valence electron count but reveals a systematic decrease with atomic number within a given group.

1. Introduction

Solid state NMR spectroscopy on diamagnetic rare earth nuclei (^{45}Sc , ^{89}Y , ^{139}La , and ^{175}Lu) within intermetallic compounds is a suitable complementary tool for structural studies, especially for cases of superstructure formation, where standard single crystal X-ray diffraction attains its limits. Meanwhile a broader data base is available for the scandium intermetallics.^{1, 2, 3} Numerous applications of ^{45}Sc solid state NMR have been published recently, illustrating the sensitivity of Knight shifts and quadrupolar coupling constants to details in the local atomic environments. Using ^{45}Sc -NMR it was possible to detect structural changes caused by thermally induced phase transitions, local defects in compounds with sub-stoichiometric site occupancies, and site multiplicities associated with superstructure formation.¹

In the case of ^{89}Y and ^{139}La NMR of intermetallic compounds, only few data are available in literature. Often, well- resolved spectra can be obtained such as for LaIr_2P_2 ⁴ and the stannides YPdSn and YPd_2Sn .⁵ Recently a comprehensive study has been published, summarizing ^{89}Y NMR spectra on more than 20 binary and ternary yttrium intermetallics. Resonance shifts vary over a wide range, from 832 ppm in YNi_2Ge_2 to 3670 ppm for elemental yttrium⁵, even though no obvious semi-empirical correlations with the structure, valence electron concentration, or the electronegativity of the bonding partners can be found when compounds with different crystal structures are being compared.

On the other hand our previous ^{45}Sc NMR work has revealed systematic Knight shift trends within certain series of isotopic compounds of composition ScTX .^{2,3} Based on these results, the present manuscript explores this question for ^{89}Y NMR within the series of YNiX and YIrX ($X = \text{Si, Ge, Sn, Pb}$) tetrelides. All of these compounds crystallize with the orthorhombic TiNiSi type structure.⁶⁻¹⁶ So far, only the structures of YNiSi ⁷ and YNiSn ¹¹ were characterized on the basis of single crystal diffraction data. YNiGe ⁸ and YNiSn ¹⁴ are Pauli paramagnets. YIrSi reveals a superconducting transition at $T_C = 2.7 \text{ K}$ ¹⁶ in addition. Herein we present single crystal data for the remaining

compounds as well as for the new stannide YIrSn. Our investigation is complemented by ^{119}Sn Mössbauer spectroscopic experiments of the YTSn stannides.

2. Experimental

Synthesis

The starting materials for the preparation of the series of YNiX ($X = \text{Si, Ge, Sn, Pb}$) and YIrX ($X = \text{Si, Ge, Sn}$) samples were yttrium ingots (smart elements), nickel wire (Johnson Matthey), iridium powder (Heraeus), lumps of silicon and germanium (Wacker), tin shots (Merck) and lead granules (ABCR GmbH) all with a stated purity better than 99.9 %. The lead granules were melted for 12 h at 770 K in an evacuated silica tube, followed by quenching and removal of the lead oxide from the surface (purification by liquation). For preparation of the YNiX ($X = \text{Si, Ge, Sn, Pb}$) samples the elements were weighed in the ideal 1 : 1 : 1 atomic ratio and arc-melted¹⁷ under an atmosphere of dried argon. All buttons were turned over and remelted several times to ensure good homogeneity. The weight losses after several meltings were in all cases < 0.5 %. The crushed buttons had a light grey color with metallic luster. They are stable in air and no decomposition was visible after several months.

The YIrX ($X = \text{Si, Ge, Sn}$) compounds were prepared *via* an induction melting process. The elements were weighed in the ideal 1 : 1 : 1 atomic ratio and arc-welded in niobium tubes under 800 mbar argon. The niobium tubes were then placed in the water-cooled sample chamber of an induction furnace (Hüttinger Elektronik, Freiburg, Germany, Typ TIG 5/300).¹⁸ The tubes were subsequently annealed for 60 min at 1900 K, followed by quenching. The samples could easily be separated mechanically from the tubes. No reaction with the crucible material could be detected. The light grey polycrystalline samples are stable in air over months.

EDX data

The single crystals studied on the diffractometers were investigated by semiquantitative EDX analyses by use of a Zeiss EVO MA10 scanning electron microscope (variable pressure mode) with Y, Ni, Ir, Ge, Sn, and PbF_2 as standards. The experimentally observed compositions were close to the ideal ones. Especially the iridium containing

crystals were carefully checked with respect to impurity phases. No contamination with the crucible material (niobium) was evident. No other impurity elements were found.

X-Ray diffraction

The polycrystalline YNiX and YIrX samples were studied by powder X-ray diffraction using a Guinier camera (equipped with an imaging plate detector, coupled with a Fujifilm BAS-1800 readout system) and $\text{CuK}\alpha_1$ radiation and α -quartz ($a = 491.30$ and $c = 540.46$ pm) as an internal standard. The orthorhombic lattice parameters (Table 1) were obtained from least-squares fits of the Guinier powder data. The correct assignment of the indices was facilitated by intensity calculations¹⁹ using the atomic positions from the structure refinements. Our experimental data are in good agreement with earlier literature data.

Small single crystals of YNiGe, YNiPb, YIrSi, YIrGe, and YIrSn were selected from the crushed annealed samples. The silvery crystals were glued to small quartz fibres using bee's wax and their quality for a diffractometer data collection was tested by Laue photographs on a Buerger camera (white Mo radiation). Intensity data of good quality crystals of YIrSi and YIrSn were collected at room temperature on a four-circle diffractometer (CAD4) with graphite monochromatized $\text{MoK}\alpha$ radiation and a scintillation counter with pulse height discrimination. Scans were taken in the $\omega/2\theta$ mode. The YIrGe crystal was measured at room temperature by use of a StoeStadiVari equipped with a Mo microfocus source and a Pilatus 100 K Detector with a hybrid-pixel-sensor. A spherical absorption correction was applied to the data set. Data for the YNiGe and YNiPb crystals were collected at room temperature by use of a Stoe IPDS-II image plate diffractometer using graphite monochromatized Mo $\text{K}\alpha$ radiation. Numerical absorption corrections were applied to these and the CAD4 data sets. All relevant details concerning the data collections and evaluations are listed in Table 2.

Structure refinements

The five diffractometer data sets showed primitive orthorhombic lattices and the systematic extinctions were compatible with space group $Pnma$, in agreement with our previous results on YPdSn.⁵ The atomic parameters of the palladium compound were taken as starting values and the structures were refined using SHELXL-97^{20, 21} (full-matrix least-squares on F^2) with anisotropic atomic displacement parameters for all

atoms. Only the YIrSi and YIrGe data sets converged with this setting. The other compounds show the reverse coloring for the polyanionic network. We subsequently interchanged the *T* and *X* sites and the refinement converged smoothly to the values listed in Tables 2 and 3. As a check for the correct composition all occupancy parameters of all data sets were refined in separate series of least-squares cycles. All sites were fully occupied within two standard deviations and in the final cycles the ideal occupancy parameters were assumed again. The final difference Fourier syntheses were flat (Table 2). The positional parameters and interatomic distances are listed in Tables 3 and 4.

Further details on the structure refinements are available. Details may be obtained from: Fachinformationszentrum Karlsruhe, D-76344 Eggenstein-Leopoldshafen (Germany), by quoting the Registry No's. CSD-427256 (YNiGe), CSD-427254 (YNiPb), CSD-427253 (YIrSi), CSD-427251 (YIrGe) and CSD-427252 (YIrSn).

⁸⁹Y solid state NMR spectroscopy

⁸⁹Y solid state NMR spectra were measured on a Bruker DSX-500 spectrometer equipped with a 7 mm low-gamma magic-angle spinning MAS-NMR probe (⁸⁹Y NMR frequency 24.5 MHz). To minimize probe detuning and rf sample heating effects of these metallic samples, intimate mixtures of the powdered material and crystalline quartz in a 1:1 mass ratio were investigated. Samples were rotated at the magic angle with rotation speeds of 5-7 kHz, and spectra were obtained in the form of Bloch decay signals, using 90° pulses of 9.5 μs length, and relaxation delays of 2-5 seconds. To suppress probe ringing effects, all the spectra were obtained following a pre-acquisition delay of one rotor period. Resonance shifts are reported relative to an external 1M aqueous YCl₃ solution.

¹¹⁹Sn Mössbauer spectroscopy

A Ca^{119m}SnO₃ source was used for the ¹¹⁹Sn Mössbauer spectroscopic investigations. The samples were placed within thin-walled PVC containers at a thickness of about 10 mg Sn/cm². A palladium foil of 0.05 mm thickness was used to reduce the tin K X-rays concurrently emitted by this source. The measurements were conducted in the usual transmission geometry at 78 K.

Electronic structure calculations

Quantum mechanical calculations on DFT level were performed using the FPLO program package (5.00-19)²² and the models of the crystal structures described in the text, the appendix and the references cited therein. As basis sets for the FPLO calculations, Y ($4s4p/5s5p4d$), Ni ($3s3p/4s4p3d$), Ir ($5s5p/6s6p5d$), Si ($2s2p/3s3p3d$), Ge ($3s3p/4s4p3d$), Sn ($4s4p/5s5p4d$) and Pb ($5s5p/6s6p5d$) functions were chosen for semicore/valence states.

3. Crystal chemistry

The equiatomic yttrium compounds YTX ($T = \text{Ni, Ir}$ and $X = \text{Si, Ge, Sn, Pb}$) crystallize with the orthorhombic TiNiSi type structure,²³ space group $Pnma$ with four formula units per cell. These structures can be considered as strongly, orthorhombically distorted variants of the aristotype AlB_2 .^{24, 25} The near-neighbor coordination for the yttrium atoms is shown in Figure 1. Each yttrium atom is coordinated by two ordered and strongly puckered T_3X_3 hexagons. Additionally these T_3X_3 hexagons show a strong tilt and we observe the formation of inter-layer $T-X$ bonds that are totally absent in AlB_2 . For all compounds, the intra- and interlayer $T-X$ bonds are close to the sum of the covalent radii,²⁶ consistent with significant $T-X$ bonding within the three-dimensional $[TX]$ networks.

The crystal chemical details of the family of TiNiSi type compounds is well documented in literature and we refer the reader to these review articles.^{24, 25, 27, 28} The YTX compounds presented here can be subdivided into two groups as a function of their coloring of the T and X atoms within the $[TX]$ network. YIrSi and YIrGe show the reverse coloring as compared to the remaining compounds. The switch of the transition metal and X positions has a drastic effect on the yttrium coordination. In the case of YIrSi and YIrGe the yttrium atoms have five nearest silicon, respectively germanium neighbors, while there are nearest transition metal neighbors in the other ones. This different coloring is not correlated with the electronegativities. However, it is obvious, that iridium is the larger atom in YIrSi and YIrGe , while the X atoms are the larger ones in YNiSi , YNiGe , YNiSn , and YNiPb . These differences in size most likely enable an effective puckering. The consequences on the ^{89}Y NMR spectra are discussed below.

4. ^{89}Y solid state NMR results and theoretical calculations

Figures 2 and 3 show the solid state NMR spectra of the YNiX and the YIrX series. While the linewidths show no systematic variations as a function of composition, there is a dependence of the isotropic signal shift on the type of the tetrelide anion. As the magnitude of the signal shift is well outside of the range of chemical shielding effects generally observed for yttrium compounds (several hundred ppm),^{29, 30} the Knight shift (K) has to be considered as dominant shift mechanism. In each case, the germanium compound shows the least pronounced Knight shift of 1450 ppm for YNiGe and 1787 ppm for YIrGe , whereas the Knight shift is maximum for the compounds with the heaviest tetrelide atom with 1796 ppm for YNiPb and 2107 ppm for YIrSn . This behavior follows a trend recently observed when the ^{45}Sc Knight shifts of the silicides ScNiX , ScPdX , and ScPtX ($X = \text{Si}, \text{Sn}$) are compared with each other: in each case, significantly higher Knight shifts are observed for the stannides as compared to the silicides.^{2,3} The dependence on atomic number observed within this group of isotypic compounds follows the electronegativities within the group-14 series. This correlation suggests a strong dependence on the electronic structure of these compounds and it was explored on the basis of DFT calculations.

The NMR signal shift of metallic compounds is in the most simple approximation direct proportional to the electronic density of states of the s -electrons at Fermi level.³⁰ ($s\text{-DOS}(E_F)$) Thus, for an estimation of the origin of the NMR signal shift³¹ quantum mechanical calculations were performed, using the models of the crystal structures described in the text. The results of these calculations are depicted in Fig. 4. A huge variation of the NMR signal shift with the $s\text{-DOS}(E_F)$ is observed instead of the linear relation expected by theory.

Additional quantum mechanical calculations were performed to rank the scattering of estimated NMR signal shifts for other Y compounds. The inset of Fig. 4 indicates a large variation of the Knight shift of the investigated compounds with respect to the $s\text{-DOS}(E_F)$. The compounds on which calculations were performed are listed in Table 6. To probe the validity of the used approximation we investigated compounds possessing multiple sites of different occupation.³³ Within this test the NMR signal shift increases with increasing $s\text{-DOS}(E_F)$ for the different sites as expected. A similar observation was obtained for the gallides of the alkaline earth metals and sodium.³⁴

To summarize the results of our investigation of the NMR signal shifts: The level of approximation used in the presented calculations is not sufficient for the description of the NMR signal shift in the investigated Y compounds. Most probably shielding contributions to the signal shift have to be included into the description. Unfortunately, no standard software is available to perform such type of calculations. Hopefully, this will change in the near future, since the general understanding of the electronic structure of intermetallic compounds has to be improved.^{35,36}

Finally, it is worth noting that spinning sideband intensity profiles indicate a magnetic shielding anisotropy of ^{89}Y in YIrSi and YIrGe. These are significantly larger than in the other compounds. This finding may be closely related to the reverse T/X site occupancy observed in these two compounds suggesting that the magnetic shielding anisotropy may be a good NMR spectroscopic indicator of this phenomenon.

6. ^{119}Sn Mössbauer spectroscopy

^{119}Sn Mössbauer spectra of the stannides YTSn ($T = \text{Ni, Rh, Ir}$) are presented in Figure 5 together with transmission integral fits. The corresponding fitting parameters are listed in Table 7 along with relevant literature data on the remaining YTSn stannides. The three spectra could be well reproduced by single quadrupole doublets in agreement with the occurrence of single crystallographic environments. The quadrupole splitting reflects the relatively low site symmetry (*m.*) of the tin atoms. Table 7 reveals that the isomer shift and quadrupole splitting parameters do not depend on the valence electron count (element group number) in a systematic fashion. On the other hand they reveal a monotonic decrease in isomer shift with increasing atomic number within the same group. As in the case of the ^{89}Y NMR results, the ^{119}Sn Mössbauer spectroscopic parameters indicate that the stannide YIrSn occupies a special position within this series of isotopic compounds.

Conclusions

Synthetic and X-ray crystallographic work confirmed the TiNiSi type structure for the series of tetrelides YTX with $T = \text{Ni, Ir}$ and $X = \text{Si, Ge, Sn, Pb}$. The coloring of the T and X atoms within the $[\text{TX}]$ network is a function of the size of T and X . On the spectroscopic side the tetrelides were characterized by ^{89}Y solid state NMR spectroscopy and the stannides in addition by ^{119}Sn Mössbauer spectroscopy. The single

yttrium sites were well detected in the ^{89}Y spectra. The Knight shifts are compared with a larger series of intermetallic yttrium compounds along with the partial electronic density of states of the 5s-like electrons at the Fermi level. These data show a very complex behavior and no simple linear dependence, indicating a multifaceted interplay of electronegativity, structure type and coloring within a given network.

Acknowledgements

We thank Dipl.-Ing. U. Ch. Rodewald for the intensity data collections. This work was financially supported by the Deutsche Forschungsgemeinschaft.

References

- 1 H. Eckert and R. Pöttgen, *Z. Anorg. Allg. Chem.* 2010, **636**, 2232 and references therein.
- 2 T. Harmening, H. Eckert, C. M. Fehse, C. P. Sebastian and R. Pöttgen, *J. Solid State Chem.* 2011, **184**, 3303.
- 3 T. Harmening, C. P. Sebastian, L. Zhang, C. Fehse, H. Eckert, R. Pöttgen, *Solid State Sci.* 2008, **10**, 1395
- 4 U. Pfannenschmidt, F. Behrends, H. Lincke, M. Eul, K. Schäfer, H. Eckert and R. Pöttgen, *Dalton Trans.* 2012, **41**, 14188.
- 5 C. Höting, H. Eckert, T. Langer, I. Schellenberg and R. Pöttgen, *J. Solid State Chem.* 2012, **190**, 216.
- 6 O. I. Bodak, V. I. Yarovets and E. I. Gladyshevskii, *Tezisy Dokl. Vses. Konf. Kristallokhim. Intermet. Soeden* 1974, 32.
- 7 E. Hovestreydt, N. Engel, K. Klepp, B. Chabot and E. Parthé, *J. Less-Common Met.* 1982, **85**, 247.
- 8 P. A. Kotsanidis, J. K. Yakinthos and E. Gamari-Seale, *J. Less-Common Met.* 1990, **157**, 295.
- 9 Y. K. Gorelenko, P. K. Starodub, V. A. Bruskov, R. V. Skolozdra, V. I. Yarovets, O. I. Bodak and V. K. Pecharskii, *Ukr. Fiz. Zh. Russ. Ed.* 1984, **29**, 867.
- 10 G. M. Koterlyn, P. K. Starodub, G. I. Kirchiv and O. I. Bodak, *Visn. Lviv Derzh. Univ. (Ser. Khim.)* 1988, 29.
- 11 M. François, B. Malaman, G. Venturini, J. Steinmetz and B. Roques, *J. Less-Common Met.* 1985, **108**, 45.
- 12 A. E. Dwight, *J. Less-Common Met.* 1983, **93**, 411.
- 13 D. Rossi, R. Marazza and R. Ferro, *J. Less-Common Met.* 1985, **107**, 99.
- 14 R. V. Skolozdra, O. E. Koretskaya and Y. K. Gorelenko, *Izv. Akad. Nauk SSSR, Neorg. Mater.* 1984, **20**, 604; *Inorg. Mater.* 1984, **20**, 520 (engl. Translation).

- 15 L. D. Gulay, Ya. M. Kalychak, M. Wołczyrz and K. Łukaszewicz, *J. Alloys Compd.* 2000, **313**, 42.
- 16 W. Xian-Zhong, B. Chevalier, J. Etourneau and P. Hagenmuller, *Mater. Res. Bull.* 1985, **20**, 517.
- 17 R. Pöttgen, Th. Gulden and A. Simon, *GIT Labor-Fachzeitschrift* 1999, **43**, 133.
- 18 R. Pöttgen, A. Lang, R.-D. Hoffmann, B. Künnen, G. Kotzyba, R. Müllmann, B. D. Mosel and C. Rosenhahn, *Z. Kristallogr.* 1999, **214**, 143.
- 19 K. Yvon, W. Jeitschko and E. Parthé, *J. Appl. Crystallogr.* 1977, **10**, 73.
- 20 G. M. Sheldrick, SHELXL-97, Program for Crystal Structure Refinement, University of Göttingen, Göttingen (Germany) **1997**.
- 21 G. M. Sheldrick, *Acta Crystallogr.* 2008, **A64**, 112.
- 22 K. Koepf, H. Eschrig, *Phys Rev. B*, 1999, **59**, 1743.
- 23 C. B. Shoemaker and D. P. Shoemaker, *Acta Crystallogr.* 1965, **18**, 900.
- 24 R.-D. Hoffmann and R. Pöttgen, *Z. Kristallogr.* 2001, **216**, 127.
- 25 E. Parthé, L. Gelato, B. Chabot, M. Penzo, K. Cenzual and R. Gladyshevskii, TYPIX–Standardized Data and Crystal Chemical Characterization of Inorganic Structure Types, Gmelin Handbook of Inorganic and Organometallic Chemistry, 8th edition, Springer, Berlin (Germany), **1993**.
- 26 J. Emsley, *The Elements*, Oxford University Press, Oxford, 1999.
- 27 G. A. Landrum, R. Hoffmann, J. Evers and H. Boysen, *Inorg. Chem.* 1998, **37**, 5754.
- 28 G. Nuspl, K. Polborn, J. Evers, G. A. Landrum and R. Hoffmann, *Inorg. Chem.* 1996, **35**, 6922.
- 29 R. Dupree and M. E. Smith, *Chem. Phys. Lett.* 1988, **148**, 41.
- 30 A. I. Becerro, A. Escudero, P. Florian, D. Massiot and M. D. Alba, *J. Solid State Chem.* 2004, **177**, 2783.
- 31 C. P. Slichter, *Principles of Magnetic Resonance*, 3rd ed., Springer, Berlin, **1990**.
- 32 F. Haarmann, *Quadrupolar NMR of intermetallic Compounds*, *eMagRes*, **2011** (DOI: 10.1002/9780470034590.emrstm1225).
- 33 C. Höting, H. Eckert, F. Haarmann, R. Pöttgen, *Z. Anorg. Allg. Chem.* submitted for publication.
- 34 F. Haarmann, K. Koch, P. Jeglič, O. Pecher, H. Rosner, Y. Grin, *Chem. Eur. J.* 2011, **17**, 7560.
- 35 R. Nesper, *Angew. Chem. Int. Ed.* 1991, **30**, 789.
- 36 Y. Grin, U. Schwarz, W. Steurer, Crystal Structure and Chemical Bonding, in: Alloy Physics: A Comprehensive Reference, Wiley-VCH, Weinheim, **2007**.
- 37 A. E. Dwight, P. P. Vaishnav, C. W. Kimball and J. L. Matykievicz, *J. Less-Common Met.* 1986, **119**, 319.

- 38 C. P. Sebastian, C. Fehse, H. Eckert, R.-D. Hoffmann and R. Pöttgen, *Solid State Sci.* 2006, **8**, 1386.
- 39 C. P. Sebastian, H. Eckert, C. Fehse, J. P. Wright, J. P. Attfield, D. Johrendt, S. Rayaprol, R.-D. Hoffmann and R. Pöttgen, *J. Solid State Chem.* 2006, **179**, 2376.
- 40 C. P. Sebastian, H. Eckert, S. Rayaprol, R.-D. Hoffmann and R. Pöttgen, *Solid State Sci.* 2006, **8**, 560.

Table 1 Refined lattice parameters (Guinier powder data) of the TiNiSi type intermetallic compounds YNiX ($X = \text{Si, Ge, Sn, Pb}$) and YIrX ($X = \text{Si, Ge, Sn}$). Standard deviations are given in parentheses.

Compound	a / pm	b / pm	c / pm	V / nm^3	Ref.
YNiSi	686.5(1)	415.4(1)	720.1(2)	0.2054	this work
	685.3	418.6	720.6	0.2067	[6]
	687.0(5)	415.5(4)	720.5(5)	0.2057	[7]
YNiGe	690.0(2)	420.3(1)	728.7(2)	0.2113	this work
	697.0(1)	421.2(1)	725.8(1)	0.2131	[9]
	687.0	421.2	725.8	0.2100	[10]
	690.2	420.1	730.2	0.2117	[8]
YNiSn	710.4(1)	444.36(8)	766.6(1)	0.2420	this work
	711.5	444.9	766.5	0.2426	[12]
	712.1(5)	442.7(2)	764.9(2)	0.2411	[14]
	713.5	444.8	767.5	0.2436	[13]
	712.6(3)	443.9(3)	767.4(2)	0.2427	[11]
YNiPb	715.0(2)	451.3(1)	775.2(2)	0.2501	this work
	715.90(4)	451.76(2)	776.10(4)	0.2150	[15]
YIrSi	678.8(3)	418.3(1)	746.4(3)	0.2119	this work
	678.9(4)	418.8(2)	746.2(6)	0.2122	[7]
	678.9	418.8	746.2	0.2122	[16]
YIrGe	683.43(8)	426.28(4)	761.98(8)	0.2220	this work
	684.3(2)	427.1(2)	761.9(3)	0.2227	[7]
YIrSn	693.6(2)	451.6(1)	796.8(3)	0.2496	this work

Table 2 Crystal data and structure refinement for YNiX ($X = \text{Ge}, \text{Pb}$) and YIrX ($X = \text{Si}, \text{Ge}, \text{Sn}$) with TiNiSi structure type, space group $Pnma$, $Z = 4$.

Empirical formula	YNiGe	YNiPb	YIrSi	YIrGe	YIrSn
Molar mass [g mol^{-1}]	220.2	354.8	309.2	353.7	399.8
Unit cell dimensions (Guinier powder data)					
a [pm]	690.0(2)	715.0(2)	678.0(3)	683.43(8)	693.6(2)
b [pm]	420.3(2)	451.3(1)	418.3(1)	426.28(4)	451.6(1)
c [pm]	728.7(2)	775.2(2)	746.4(3)	761.98(8)	796.8(3)
Cell volume [nm^3]	0.2113	0.2501	0.2119	0.2220	0.2496
Calculated density [g cm^{-3}]	6.92	9.42	9.69	10.58	10.64
Crystal size [μm^3]	$20 \times 20 \times 60$	$20 \times 20 \times 70$	$40 \times 60 \times 120$	$40 \times 40 \times 40$	$20 \times 20 \times 80$
Transm. ratio (max / min)	0.65 / 0.22	0.38 / 0.05	0.14 / 0.04	0.25 / 0.06	0.43/0.16
Diffractometer	IPDS II	IPDS II	CAD4	StadiVari	CAD4
Detector distance [mm]	60	60	–	50	–
Exposure time [sec]	300	240	–	28	–
ω range; increment [$^\circ$]	0-180; 1.0	0-180; 1.0	–	–; 0.3	–
Integration parameters A,B, EMS	12.8, 2.9, 0.012	12.9, 2.7, 0.01	–	7.0, –5.2, 0.012	–
Absorption coefficient [mm^{-1}]	49.7	97.2	90.0	98.7	85.8
$F(000)$ [e]	396	596	520	592	664
θ range [deg]	4.1–34.9	3.9–34.9	4.1–40.0	4.0–40.4	3.9–39.9
Range in hkl	$\pm 10, \pm 6, \pm 11$	$\pm 11, \pm 7, \pm 12$	$\pm 12, \pm 7, \pm 13$	$\pm 12, \pm 7, \pm 13$	$\pm 12, \pm 8, \pm 14$
Total no. reflections	1688	2021	4948	2149	4264
Independent reflections / R_{int}	509 / 0.0593	609 / 0.0538	723 / 0.0422	744 / 0.0636	842 / 0.0613
Reflections with $I \geq 2\sigma(I)$	215 / 0.0844	451 / 0.0362	665 / 0.0091	626 / 0.0224	669 / 0.0312
Data / parameters	509 / 20	609 / 20	723 / 20	744 / 20	842 / 20
Goodness-of-fit on F^2	0.64	1.45	1.71	1.82	1.16
$R1 / wR2$ for $I \geq 2\sigma(I)$	0.0198 / 0.0380	0.0304 / 0.0650	0.0181 / 0.0237	0.0300 / 0.0714	0.0250 / 0.0449
$R1 / wR2$ for all data	0.0688 / 0.0439	0.0479 / 0.0674	0.0211 / 0.0241	0.0352 / 0.0722	0.0428 / 0.0495
Extinction coefficient	150(9)	37(8)	79(7)	131(12)	132(5)
Largest diff. peak / hole, [$\text{e} / \text{Å}^{-3}$]	3.00/ –3.08	4.34 / –3.86	4.23 / –2.79	5.33 / –4.04	3.58 / –3.05

Table 3 Atomic positions and anisotropic displacement parameters (pm^2) of YNiX ($X = \text{Ge}, \text{Pb}$) and YIrX ($X = \text{Si}, \text{Ge}, \text{Sn}$), space group $Pnma$. The anisotropic displacement factor exponent takes the form: $-2\pi^2[(ha^*)^2U_{11} + \dots + 2hka^*b^*U_{12}]$; $U_{12} = U_{23} = 0$; U_{eq} is defined as one third of the trace of the orthogonalized U_{ij} tensor. All atoms lie on Wyckoff sites $4c$ ($x \ 1/4 \ z$).

Atom	x	z	U_{11}	U_{22}	U_{33}	U_{13}	U_{eq}
YNiGe							
Y	0.0060(3)	0.70747(8)	53(3)	62(2)	71(3)	1(1)	62(2)
Ni	0.3095(3)	0.4205(2)	112(7)	79(6)	73(7)	1(1)	88(4)
Ge	0.2006(2)	0.0896(2)	80(5)	40(5)	42(4)	0(1)	54(3)
YNiPb							
Y	0.0093(2)	0.7071(2)	88(5)	110(5)	116(5)	4(4)	105(3)
Ni	0.2971(3)	0.4177(3)	185(7)	109(6)	133(7)	13(10)	142(4)
Pb	0.19774(8)	0.08790(7)	114(2)	79(2)	106(2)	0(1)	100(1)
YIrSi							
Y	0.00526(6)	0.68691(6)	45(2)	81(2)	40(2)	-6(1)	55(1)
Ir	0.15643(2)	0.06423(2)	45(1)	69(1)	39(1)	3(1)	51(1)
Si	0.2984(2)	0.3898(2)	48(5)	61(5)	66(5)	0(1)	58(3)
YIrGe							
Y	0.0075(1)	0.6909(1)	137(3)	136(3)	130(3)	-1(1)	135(2)
Ir	0.15963(5)	0.06349(5)	137(1)	125(1)	130(1)	3(1)	131(1)
Ge	0.2917(2)	0.3882(2)	135(4)	118(3)	142(4)	0(1)	132(2)
YIrSn							
Y	0.0186(1)	0.6912(1)	69(3)	79(3)	86(3)	0(1)	78(2)
Ir	0.27143(5)	0.39744(4)	83(1)	62(1)	77(1)	3(1)	74(1)
Sn	0.16833(8)	0.07396(6)	84(2)	59(2)	70(2)	3(2)	71(1)

Table 4 Interatomic distances (pm) in the structures of YNiX ($X = \text{Ge, Pb}$) and YIrX ($X = \text{Si, Ge, Sn}$). Standard deviations are all equal or less than 0.3 pm. All distances within the first coordination spheres are listed.

YNiGe			YNiPb			YIrSi			YIrGe			YIrSn		
Y:	2 Ni	290.6	Y:	1 Ni	304.4	Y:	2 Si	290.6	Y:	2 Ge	294.7	Y:	1 Ir	292.5
	2 Ge	293.9		2 Ni	311.0		1 Si	297.9		2 Ge	301.4		2 Ir	310.5
	1 Ni	295.9		2 Pb	313.2		2 Si	299.2		1 Ge	301.5		2 Ir	315.0
	1 Ge	302.1		1 Pb	319.2		1 Ir	299.7		1 Ir	302.4		2 Sn	320.6
	1 Ni	303.1		2 Pb	321.5		2 Ir	300.5		2 Ir	305.8		1 Sn	321.9
	2 Ge	304.2		1 Pb	324.5		1 Ir	302.0		1 Ir	306.7		1 Sn	322.2
	1 Ge	309.1		1 Ni	328.1		2 Ir	323.8		2 Ir	326.5		2 Sn	326.9
	2 Ni	316.6		2 Ni	329.0		1 Si	345.7		1 Ge	353.0		2 Y	359.2
	2 Y	350.5		2 Y	363.6		2 Y	348.8		2 Y	353.4		1 Ir	369.9
	2 Y	368.3		2 Y	392.7		2 Y	352.2		2 Y	360.8		2 Y	380.1
Ni:	2 Ge	243.7	Ni:	2 Pb	261.4	Ir:	1 Si	245.4	Ir:	2 Ge	253.7	Ir:	1 Sn	267.5
	1 Ge	252.6		1 Pb	265.3		2 Si	248.3		1 Ge	254.1		2 Sn	269.3
	1 Ge	270.0		1 Pb	286.5		1 Si	261.4		1 Ge	263.3		1 Sn	276.2
	2 Y	290.6		1 Y	304.4		1 Y	299.7		1 Y	302.4		1 Y	292.5
	1 Y	295.9		2 Y	311.0		2 Y	300.5		2 Y	305.8		2 Y	310.5
	1 Y	303.1		1 Y	328.1		1 Y	302.0		1 Y	306.7		2 Y	315.0
	2 Y	316.6		2 Y	329.0		2 Ir	313.1		2 Ir	320.0		1 Y	369.9
	2 Ni	355.9		2 Ni	389.1		2 Y	323.8		2 Y	326.5		2 Ir	418.9
Ge:	2 Ni	243.7	Pb:	2 Ni	261.4	Si:	1 Ir	245.4	Ge:	2 Ir	253.7	Sn:	1 Ir	267.5
	1 Ni	252.6		1 Ni	265.3		2 Ir	248.3		1 Ir	254.1		2 Ir	269.3
	1 Ni	270.0		1 Ni	286.5		1 Ir	261.4		1 Ir	263.3		1 Ir	276.2
	2 Y	293.9		2 Y	313.2		2 Y	290.6		2 Y	294.7		2 Y	320.6
	1 Y	302.1		1 Y	319.2		1 Y	297.9		2 Y	301.4		1 Y	321.9
	2 Y	304.2		2 Y	321.5		2 Y	299.2		1 Y	301.5		1 Y	322.2
	1 Y	309.1		1 Y	324.5		1 Y	346.7		1 Y	353.0		2 Y	326.9

Table 5 ^{89}Y MAS NMR isotropic resonance shifts ($\delta_{\text{iso}} \pm 2$ ppm) and Full widths at half height ($\Delta \pm 10$ Hz) of YNiX ($X = \text{Si, Ge, Sn, Pb}$) and YIrX ($X = \text{Si, Ge, Sn}$).

Compound	δ_{iso} (ppm)	Δ (Hz)	Ref.
YNiSi	1524	753	[5]
YNiGe	1450	520	[5]
YNiSn	1640	370	[5]
YNiPb	1796	922	this work
YIrSi	1837	605	[5]
YIrGe	1787	122	this work
YIrSn	2107	2326	this work

Table 6 Intermetallic compounds used for quantum mechanical calculations. The NMR signal shifts and electronic density of states at the Fermi level ($s\text{-DOS}(E_F)$) are given for a multiplicity of compounds in different structure types.

Compound	Structure type	Signal shift (ppm)	$s\text{-DOS}(E_F)$
YMg	CsCl	2923	0.008
YCu	CsCl	2851	0.051
YZn	CsCl	1600	0.004
YAg	CsCl	2923	0.046
YAu	CsCl	2794	0.081
YCoC	YCoC	1486	0.022
YCo ₂ Si ₂	ThCr ₂ Si ₂	1521	0.004
YNi ₂ Si ₂	ThCr ₂ Si ₂	756	0.012
YCu ₂ Si ₂	ThCr ₂ Si ₂	585	0.004
YRu ₂ Si ₂	ThCr ₂ Si ₂	2131	0.012
YRh ₂ Si ₂	ThCr ₂ Si ₂	1278	0.007
YPd ₂ Si ₂	ThCr ₂ Si ₂	1013	0.014
YNi ₂ Ge ₂	ThCr ₂ Si ₂	832	0.005
YRh ₂ Si	YRh ₂ Si	1416	0.006
		2995	0.097
Y ₂ RhSi ₃	Lu ₂ CoGa ₃	669	0.005
		1376	0.097
YCuSi	ZrBeSi	1386	0.016
YAgSi	ZrNiAl	1445	0.011
YAgGe	ZrNiAl	1480	0.010
YRhSn	ZrNiAl	2087	0.089
YNiSi	TiNiSi	1524	0.040
YNiGe	TiNiSi	1450	0.027
YIrGe	TiNiSi	1787	0.021
YNiSn	TiNiSi	1640	0.045
YPdSn	TiNiSi	1440	0.045
YIrSn	TiNiSi	2107	0.088
YNiPb	TiNiSi	1796	0.036
YCuSn	NdPtSb	2045	0.026
YAgSn	NdPtSb	2152	0.032
YCuPb	LiGaGe	2182	0.026
YRh ₂ Sn	MnCu ₂ Al	3194	0.011
YPd ₂ Mg	MnCu ₂ Al	3874	0.026
YPd ₂ Cd	MnCu ₂ Al	3802	0.020
YPd ₂ Sn	MnCu ₂ Al	1920	0.007

Table 7 Fitting parameters of ^{119}Sn Mössbauer spectroscopic measurements of the series of YNiX ($X = \text{Si, Ge, Sn, Pb}$) and YIrX ($X = \text{Si, Ge, Sn}$): isomer shift (δ_{iso}), electric quadrupole interaction (ΔE_Q) and experimental line width (Γ). Numbers in parentheses represent the statistical errors in the last digit.

Compound	δ (mm/s)	ΔE_Q (mm/s)	Γ (mm/s)	Ref.
YCoSn	1.78(1)	0.50(2)	1.01(3)	[37]
YRhSn	1.75(1)	0.68(2)	1.04(3)	this work
YIrSn	1.70(1)	0.97(1)	1.09(1)	this work
YNiSn	1.82(1)	0.83(2)	1.07(3)	this work
YPdSn	1.78(1)	0.90(1)	1.10(3)	[5]
YCuSn	1.80(3)	0.61(1)	0.94(1)	[38]
YAgSn	1.78(1)	0.43(4)	0.91(9)	[39]
YAuSn	1.72(3)	0.62(1)	0.89(2)	[40]

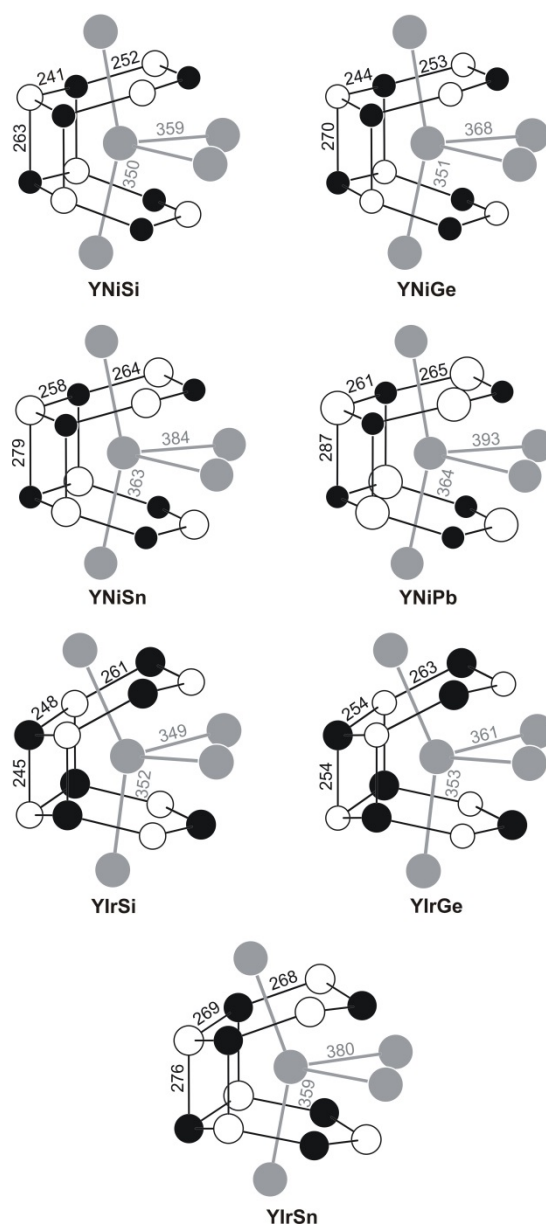


Fig. 1 The near neighbor coordination of yttrium in the structures of YNiX ($X = \text{Si}, \text{Ge}, \text{Sn}, \text{Pb}$) and YIrX ($X = \text{Si}, \text{Ge}, \text{Sn}$). Yttrium, nickel (iridium) and the group IV elements are drawn as medium grey, black filled and open circles, respectively. Relevant interatomic distances (pm) are indicated.

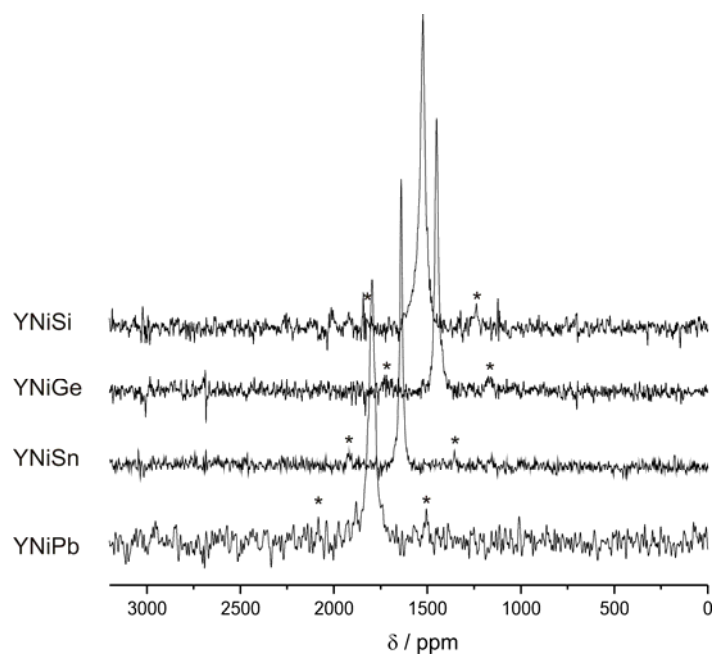


Fig. 2 24.5 MHz solid state NMR spectra of the YNiX ($X = \text{Si}, \text{Ge}, \text{Sn}, \text{Pb}$) series at room temperature. Spinning sidebands are marked by asterisks.

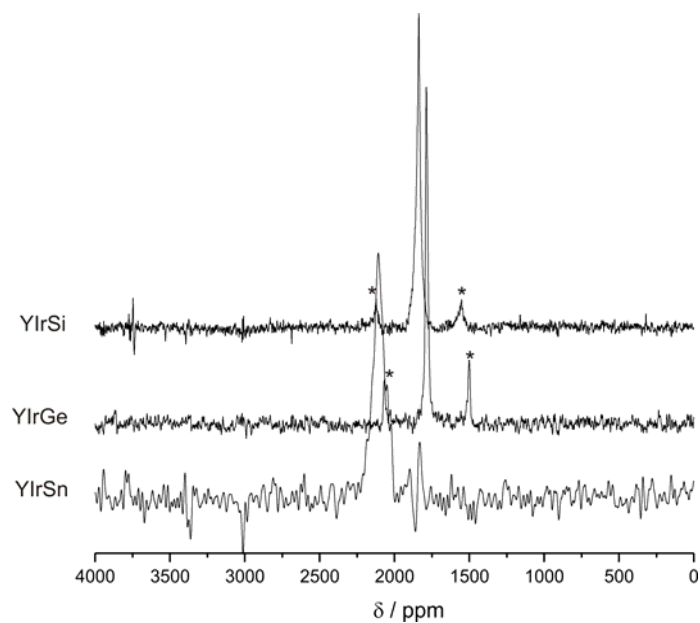


Fig. 3 24.5 MHz solid state NMR spectra of the YIrX ($X = \text{Si}, \text{Ge}, \text{Sn}$) series at room temperature. Spinning sidebands are marked by asterisks.

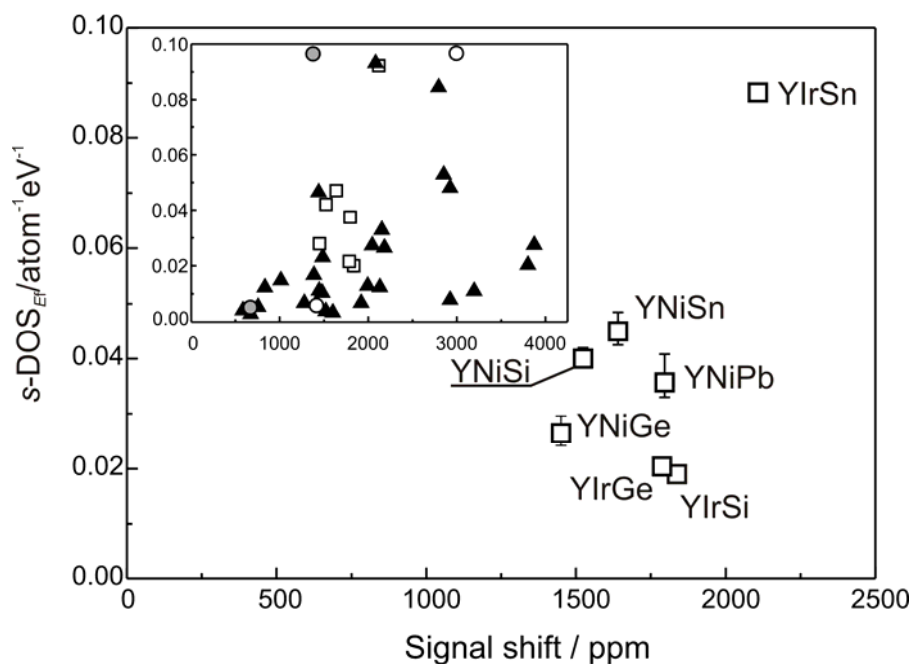


Fig. 4 Partial electronic density of states of the 5s-like electrons at the Fermi level ($s\text{-DOS}(E_F)$) versus NMR signal shift of the ^{89}Y isotope. Main panel: TiNiSi type structure compounds. Inset: Squares (\square) represent the TiNiSi type compounds. Other symbols originate from varying compounds: filled triangles (\blacktriangle), open (\circ) and grey filled (\bullet) circles emerge from YRh_2Si and Y_2RhSi_3 , respectively.

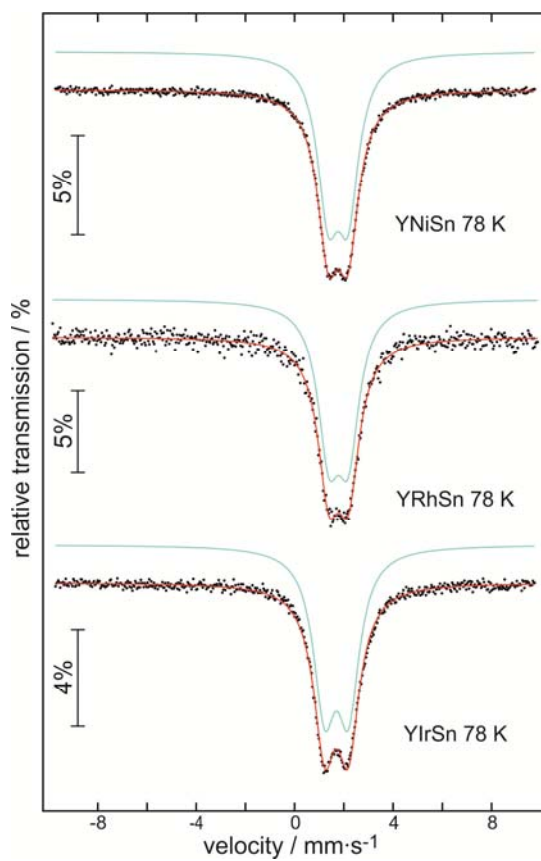


Fig. 5 Experimental (data points) and simulated (continuous lines) ¹¹⁹Sn Mössbauer spectra of YNiSn, YRhSn and YIrSn at 78K.